



# The effect of welding current on nugget geometry, microstructure and mechanical properties of TWIP steels in resistance spot welding

Sadettin Şahin<sup>1</sup> · Fatih Hayat<sup>2</sup> · Onur Cem Çölgeçen<sup>2</sup>

Received: 2 November 2020 / Accepted: 26 January 2021 / Published online: 13 February 2021  
© International Institute of Welding 2021

## Abstract

In this study, two twinning induced plasticity (TWIP) steels with different chemical compositions were produced by casting-hot rolling-cold rolling processes. A total of four groups of samples were formed by obtaining cold-rolled and heat-treated samples giving optimum mechanical properties. Welding parameters of resistance spot welding (RSW) of all samples were determined, and weldability at different welding current values was examined. Button shapes, microstructures, microhardness, and tensile shearing tests of welded joints were investigated. In addition, scanning electron microscopy (SEM) and energy dispersive X-ray (EDX) analyses of broken samples were examined as a result of tensile testing. It has been concluded that non-heat-treated samples have higher tensile strength than heat-treated samples. In heat-treated steels; a marked increase in ductility was observed. It has been observed that RSWs of non-heat-treated steels have higher tensile load bearing capacity (TLBC) value.

**Keywords** AHSS · TWIP steel · Resistance spot welding · Welded joints · Tensile shear strength · SEM

## 1 Introduction

According to the data of the International Organization of Motor Vehicle Manufacturers (OICA), the global production amount is 95,634,593 vehicles in 2018. Number of automobiles are 70,498,388 and the remainder are commercial vehicles. Steel is used to construct a car's chassis and body, including the roof, body, door panels, and the beams between doors. Steel is often used in mufflers and exhaust pipes. Technological advances over the years have enabled

automakers to utilize different types of steel with varying levels of rigidity [1].

Using high-strength materials is becoming increasingly important in the automotive industry. In the last 30 years, a great variety of high strength steels have been developed for this purpose. In order to accommodate increasing safety and environmental requirements, innovative lightweight designs require the manufacture of complex components with greater strength and lower weight [2]. TWIP steels are a new class of steel grade and a representative of lightweight materials. Due to their alloy composition, they are able to combine the conflicting goals of high strength and high elongation [3–8].

In recent years, particular importance has been attached to austenitic Fe-Mn steels for applications in automotive vehicle structures [9].

Automaker has shown preferences on twinning induced plasticity (TWIP) steels, which have superior strength and ductility compared to other AHSS [10, 11]. The novel fully austenitic Fe-Mn steels with a Mn content between 15 and 25% exhibit great potential in terms of their unusual combination of high ductility and strength [12]. TWIP steel could lead to an effective reduction of the specific weight of these steels (6.8–7.3 g/cm<sup>3</sup>, depending on Al content), which is particularly significant to the automobile industry and makes less carbon emission and

---

Recommended for publication by Commission III - Resistance Welding, Solid State Welding, and Allied Joining Process

---

✉ Fatih Hayat  
fhatay@karabuk.edu.tr

Sadettin Şahin  
ssahin@kku.edu.tr

Onur Cem Çölgeçen  
occolgecen@akplas.com

<sup>1</sup> Metallurgy Materials Engineering Department, Engineering Faculty, Kırıkkale University, Kırıkkale, Turkey

<sup>2</sup> Metallurgy Materials Engineering Department, Engineering Faculty, Karabuk University, Karabuk, Turkey

fuel consumption possible. Thus, the industrial focus is now mainly on TWIP steels of Fe-Mn-C-Al and Fe-Mn-Si-Al alloy systems [13, 14]. Especially, the resulting high energy-absorption capacity makes these steels suitable for applications such as crash relevant structural components in automobiles, which are expected to dissipate the kinetic energy during a crash incident by deforming plastically [15].

Thousands of parts are used in the production of an automobile and hundreds of different types of processes are performed. Perhaps, the most important of these processes are the welding processes that affect the vehicle quality by 40% and the body of the vehicle is revealed. In automobile manufacturing, welding is one of the most important factors affecting the lifespan, safety, endurance, and quality of a vehicle. Resistance spot welding (RSW), the primary method used to join vehicle, automotive structural components, is accomplished through a combination of heat, pressure, and time [16–20]. RSW uses the application of electric current and mechanical pressure to create a weld between two pieces of metal. Weld electrodes conduct the electric current to the two pieces of metal as they are forged together [21–24]. Advantages of the spot welding technique are that it is relatively fast, robust, and economic. It is a known fact that 3000–5000 resistance spot weld processes are performed in manufacturing an automobile [25, 26]. In large vehicles, approximately 20,000 resistance spot welding process is applied.

There are studies in the literature about welded joints of TWIP steels. Some of them can be given as follows. Laser welding [27–33], resistance spot welding [34–39], TIG welding [27, 40], MAG [41], etc. many applications have been seen in the literature. In this study, microstructure, SEM, EDX analysis, microhardness, and tensile test of the spot weld joints of low and medium carbon TWIP steels with medium manganese were investigated.

## 2 Experimental procedure

In this study, a special production sheet of two TWIP having 2.5 mm thickness in cold-rolled condition produced was used. The measured chemical compositions of these steels are shown in Table 1.

**Table 1** Chemical composition (mass%)

	C	Mn	Si	Cr	S	Fe
TWIP1	0.10	xxx	1.52	0.18	< 0.005	Balanced
TWIP2	0.30	xxx	0.6	0.05	< 0.005	Balanced

Test specimens were melted by induction melting in a furnace casted as bar. These bars were homogenized at 1200 °C for 6 h and hot-rolled to a plate at the temperatures between 1100 and 1000 °C. After hot rolling the specimens were 40% cold rolled. The heat treatment was carried out at 800 °C and air-cooling applied for all specimens. RSW was applied to the samples prepared in 4 groups. The codes and abbreviations given to the samples are as follows: TWIP1: steel in the first chemical composition, TWIP1-H: heat-treated version of the first alloy, TWIP2: steel in the second chemical composition, TWIP2-H: heat-treated version of the second alloy. In the heat treatment results of cold-rolled samples, temperatures giving the highest mechanical properties were chosen. This temperature was determined as 800 °C.

Specimens were cut into 100 × 30 mm pieces. Specimens were welded by using a pneumatic phase-shift controlled RSW machine, and an AC spot welding machine, with a capability of a 0–30 kA effective weld current and a capacity of 120 kVA. Before joining, the surface of the test pieces was cleaned mechanically and then welded using a conical water-cooled electrode from a Cu – Cr alloy. The diameter of the contact surface of the electrode was 8.0 mm. For joining, 30 cycles (1 cycle = 0.02 s.), welding time was applied, while other welding parameters such as the weld currents 5, 7, 9, 11, and 13 kA. Electrode pressure ( $6 \times 10^5$  Pa), and the holding time of the electrode (20 cycles) was kept constant (weld atmosphere; ambient).

The tensile shear load bearing capacity (TLBC) values of the welded samples were determined. The test samples conform to the specification DIN 40 120. The TLBC of welded materials was determined by using a microprocessor-controlled Shimadzu UH type servo hydraulic universal testing machine.

The Vickers micro hardness measurement across the weld metal and heat-affected zone (HAZ) and of the base metal was carried out on the metallographic specimens with a load of 200 g. The nugget diameter, nugget height, and immersion depth of welded joints were measured by using a caliper with a sensitivity of 1/100 mm.

The transverse sections of the weld passing through the weld nugget as well as the similar section of the base metal were prepared. The cross section of the weld joints and base metal were ground with SiC papers up to 2000 grit followed by polishing using 3 and 1 μm diamond paste. The polished samples were etched with 3% Nital (3% HNO<sub>3</sub> in ethanol) solution for metallographic observations. A Zeiss Model optical microscope was used to observe the microstructure.

Thereafter, the welds and fracture pieces were cut in cross-section and investigations were carried out by SEM. Optical examination of samples was carried out by using a Zeiss microscope. The fracture surfaces were analyzed by SEM and EDX analyses.



**Fig. 1** TWIP1 steel welded with 11 kA. **a, b** Main metal and heat-affected zone (HAZ). **c, d** Dendrite and interdendritic region

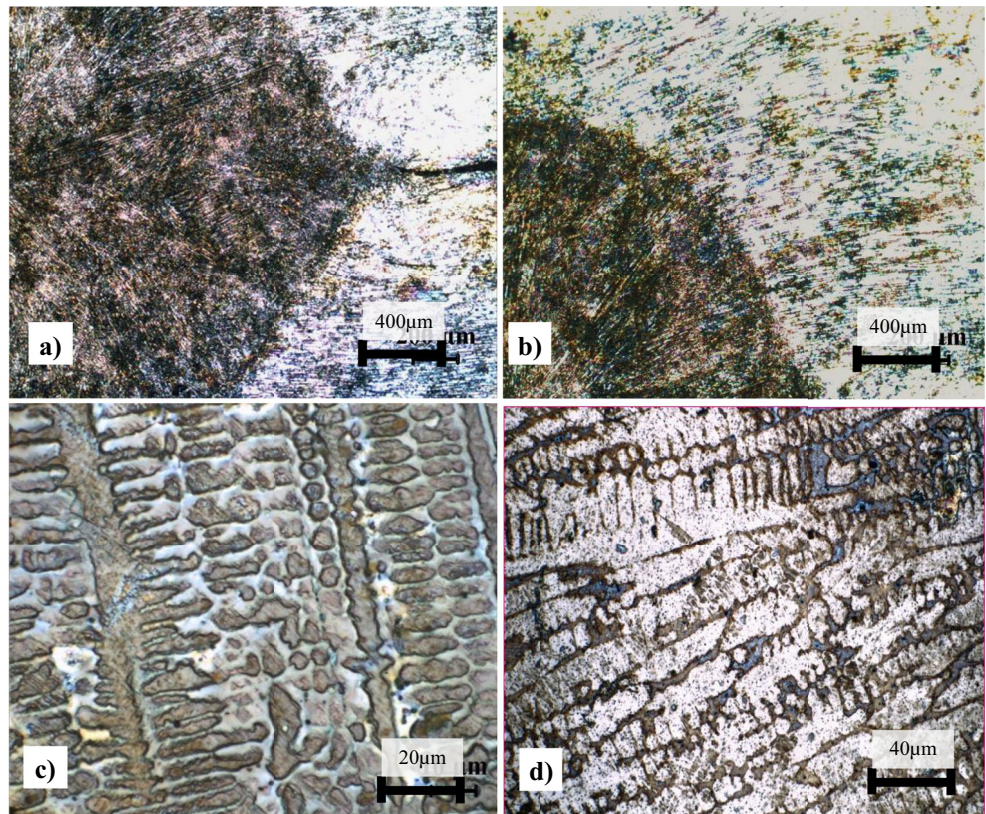


**Fig. 2** TWIP 2 steel welded with 9 kA. **a, b** Main metal and HAZ. **c, d** Weld pool (columnar dendrites and Mn segregation images)

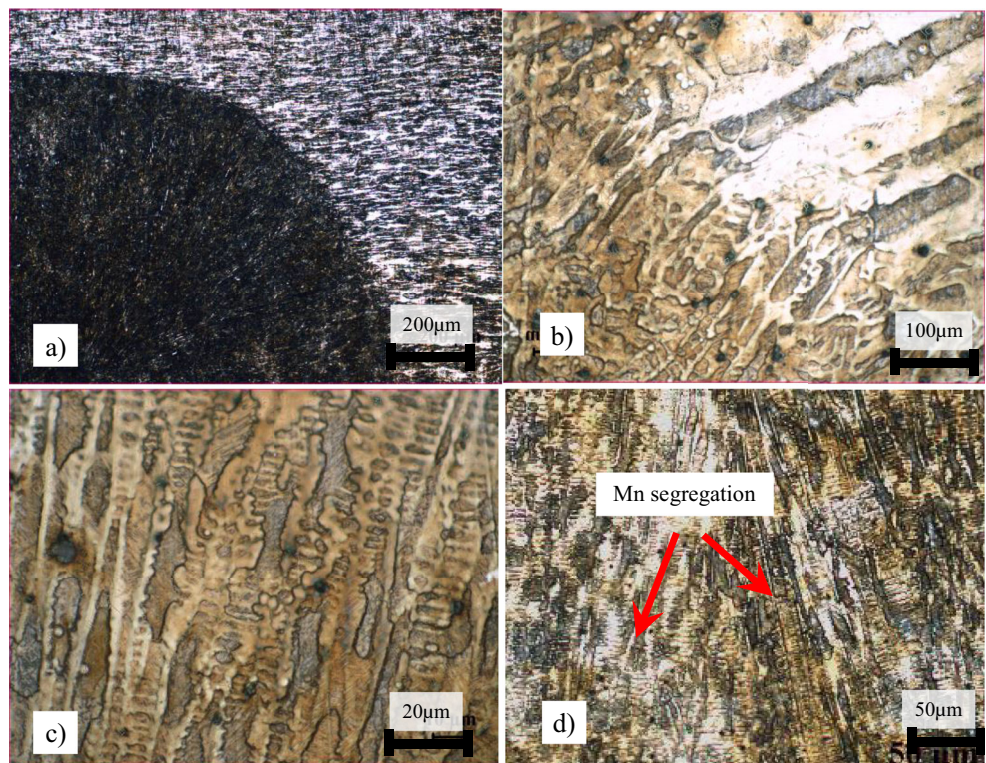
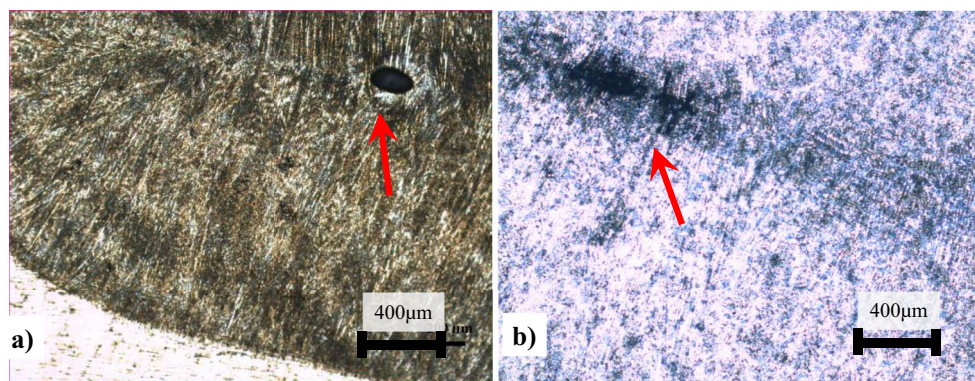




**Fig. 3** Macro shrinkage pores in the nucleus region welded with 13 kA. **a** TWIP2, **b** TWIP2-H



### 3 Results and discussion

#### 3.1 Microstructure and mechanical properties

The microstructure of sheets in the initial state (annealed after cold rolling) is very complex.  $\epsilon$  martensite colourless  $\gamma$  (austenite) and  $\alpha'$  martensite. After heat treatment of TWIP1 and TWIP2 alloys, austenitic structure and twinning have been determined. Kang Singon et al. reported that in a study of TWIP steels (Fe – 18Mn – 0.6C – 1.5Al) with close Mn values, carbides were formed between 700 and 800 °C [42]. They stated that these carbide formations were dissolved at 800 °C and that only the twinned austenite microstructure was formed. Twinning mechanisms normally obtained as a result of deformation reach a more clear and regular orientation as a result of heat treatment. In the preliminary studies of these alloys, it was observed that carbides disappear at temperatures of 800 °C and above, and grains containing a completely austenitic microstructure twinning mechanism remain.

In addition, as a result of tensile tests, the heat treatment temperatures of the samples to be welded were determined as 800 °C. The mechanical properties of the samples to be welded were determined as follows: tensile strength of TWIP1 steel is 1675 MPa, yield strength is

1300 MPa elongation value is 18%. The tensile strength of the heat-treated (TWIP1-H) sample is 1220 MPa, the yield strength is 356 MPa, and the elongation value is 44%. Tensile strength of TWIP2 steel is 1505 MPa, yield strength is 1495 MPa, and elongation value is 14.5%. The tensile strength of the heat-treated (TWIP2-H) sample is 1180 MPa, the yield strength is 345 MPa, and the elongation value is 55%. Resistance spot welding process was carried out on these samples.

#### 3.2 Microstructure of welded joints

Microstructure changes of TWIP1 and TWIP2 steels are shown in Figs. 1 and 2.

TWIP steels are austenitic because of their enough manganese content. In the welded connection, the base metal consists of HAZ and the welding nucleus consists of the austenite phase. Grain growth was observed in HAZ due to thermal cycles. Grain size was larger and more complex than basic metal. The final structure in the weld metal consists of dendrite morphology directed towards the melting center during melting from melting temperature to room temperature.

Considering the welding parameters, macro shrinkage gaps were found in the nucleus of the connections originating at 13 kA. Due to the shrinkage that occurs during

**Fig. 4** Insufficient joining region and weld in 3-kA welding current

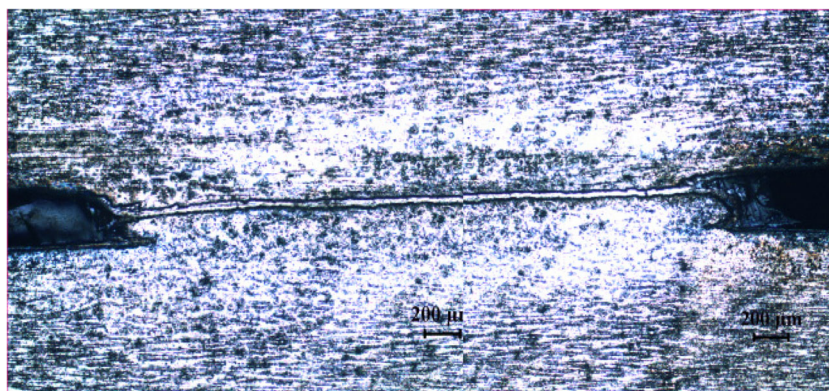
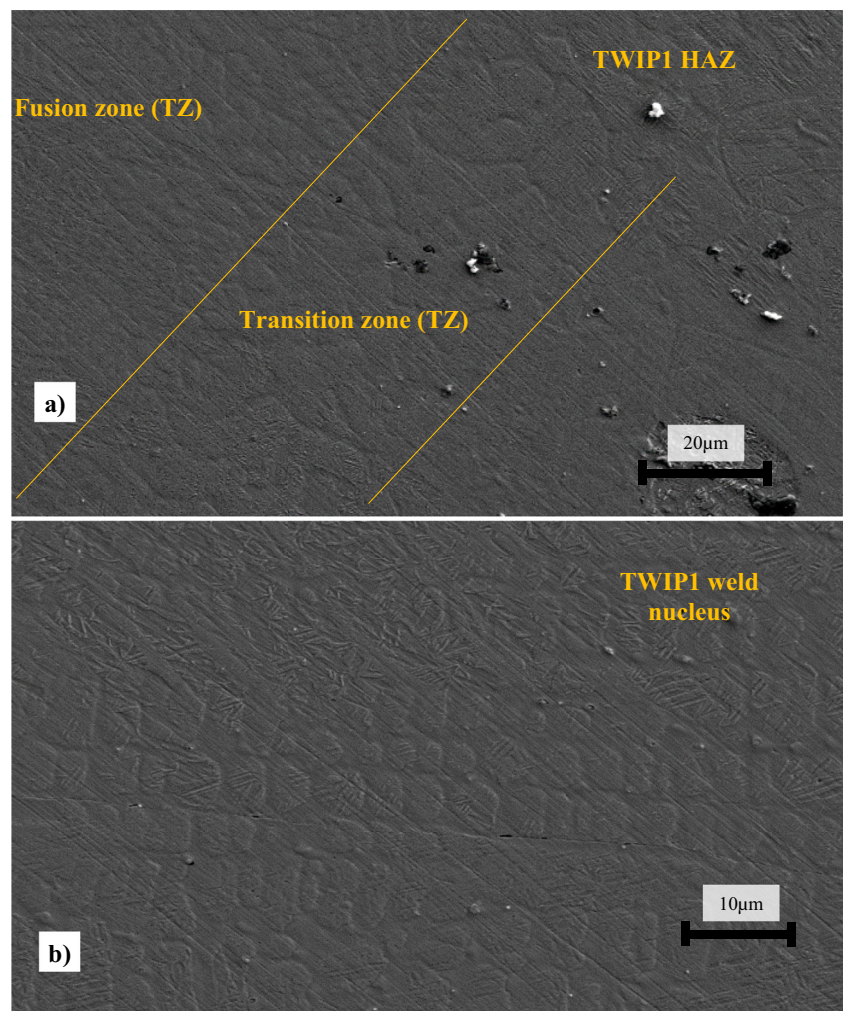


**Fig. 5** SEM displays of TWIP1 welded samples: **a** Transition zone, **b** weld nucleus



solidification, micro pores-gaps are formed between the dendrites. With the increasing solidification rate of the weld metal of TWIP steels, the possibility of micro pore formation will increase. This is due to the high shrinkage tendency and high tensile properties of TWIP steels. For this reason, heating will increase at high welding parameters, while cooling rate will increase and as a result, gap formation will increase, and the weld metal mass will decrease. In addition, high heat input caused by high current value during welding process will cause excessive melting and spattering, thus triggering the formation of voids. In Fig. 3, macro shrinkage gaps caused by high welding current are shown.

Macro pores (gap) were not detected in samples with TWIP1 coding but it was seen in TWIP1-H. These results showed that the 13-kA welding current was not suitable. In addition, it was determined that the nucleus did not form due to insufficient melting of the welded connections made in 3 kA (Fig. 4). For this reason, joints with 3-kA welding current have not been tested.

### 3.3 SEM/EDS analysis results of welded joints

HAZ, weld nucleus SEM photographs of TWIP1, and TWIP2 coded welded samples are given in Figs. 5 and 6.

The figures show twinning zones formed on base metal. Also, melting zone and partial melting zone are shown. Base metal, HAZ, weld nucleus SEM photographs, and EDS analysis of TWIP1-H welded samples are given in Fig. 6.

HAZ and weld nucleus SEM photographs of TWIP2 non heat-treated welded samples are given in Fig. 7.

As seen in Fig. 7, primary dendrites and dendrite arms are constantly and integratedly joined in the welding nucleus. There are pores in the welding nucleus. Shrinkage porosities trigger formation of micro-pores and are thought to occur at the final stage of solidification. It is believed that the cooling rate paves the way for the increase of shrinkage pores. The proportion of pores also increases due to the high heat input compared to the low heat input.

Base metal, HAZ, and weld nucleus SEM photos of TWIP2 heat-treated (TWIP2-H) welded samples are given in



**Fig. 6** SEM displays and EDX analyses of TWIP1-H welded samples

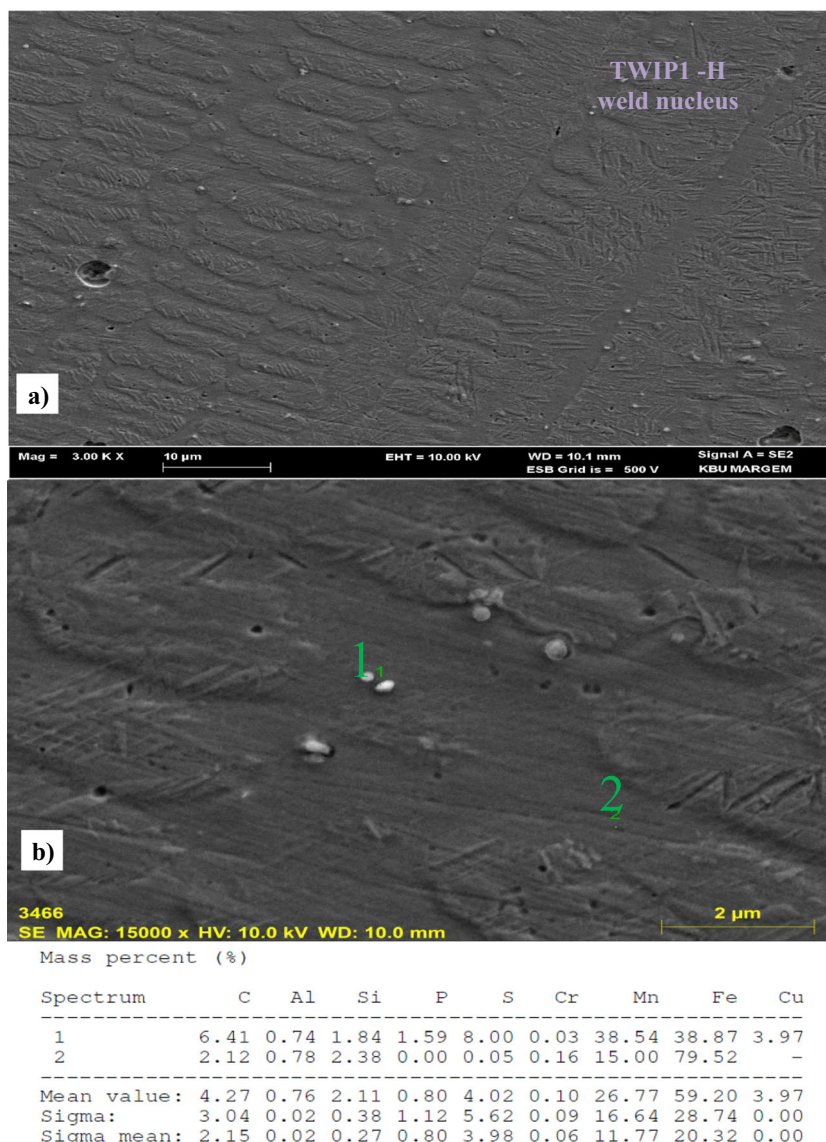


**Fig. 8.** EDS analysis was performed to determine the difference of chemical composition in the melting zone. Primary dendrites and dendrite arms were examined.

The transformation of the grains ( $L \rightarrow \gamma + M_3C$ ) occurs as a result of the solidification of the melting region of Fe and Mn carbides ( $(Fe, Mn)_3C$ ) by the eutectic reaction. J. Yoo et al. [43] reported that Fe and phosphorous formed  $Fe_2P$  in the region between the dendrites as a result of solidification of melting zone of TWIP980 steel in the GTAW and laser welding process.

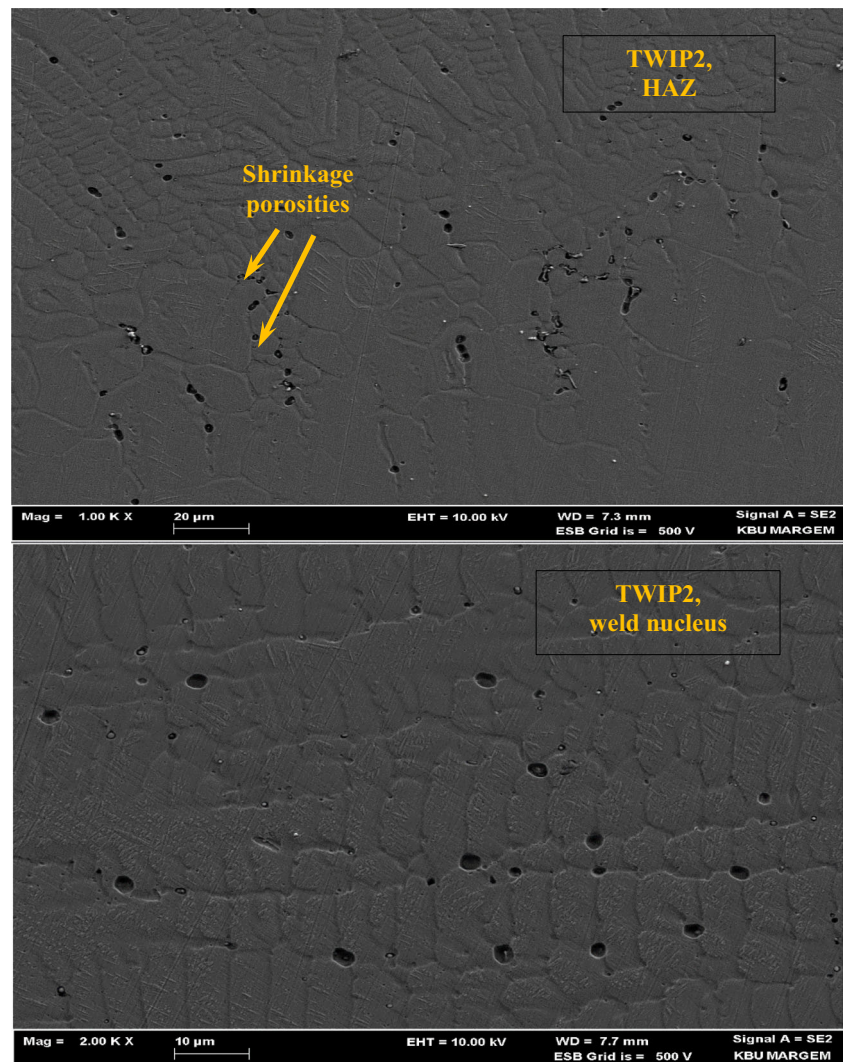
Similar results were found in this study. While the P ratio in dendrite (dendritic) structure is 0% at point 2 of EDS results, in precipitate number 1, (precipitate) P ratio reached approximately 0.9%. In addition, the Mn ratio was at 14.10% in region 2 and increased to 24.48% at region 1. There was also a 4-fold increase in element C. Similarly, Tao Wang et al. [31] in their study reported the dendrites in the weld metal of TWIP

steel laser welding. In primary dendrites, while C and Mn are relatively low, this rate increased between the dendrite arms, and reached the highest level in the interdendritic region. They reported that the increase in the ratio of Mn and C was higher towards the boundaries of the dendrite grains. According to the EDS analysis, the carbon % ratio increased from 0.59 to 0.83% (wt.%). The percentage of Mn increased from 16.6 to 22.86% (wt.%).

### 3.4 Weld nugget geometry

A difference was observed in the increase of the nugget diameter as a result of the welded joint in the experiments. The images of the nugget diameters are given in Table 2. Table 3 shows the nugget diameter, nucleus, and indentation depth of welded samples.

**Fig. 7** SEM displays of TWIP2 welded samples



According to the results obtained, HAZ widths are close to each other. Nugget diameters were smaller in heat-treated samples. In the depth measurement, low values were also determined in the samples that were heat treated.

### 3.5 Tensile shear test results

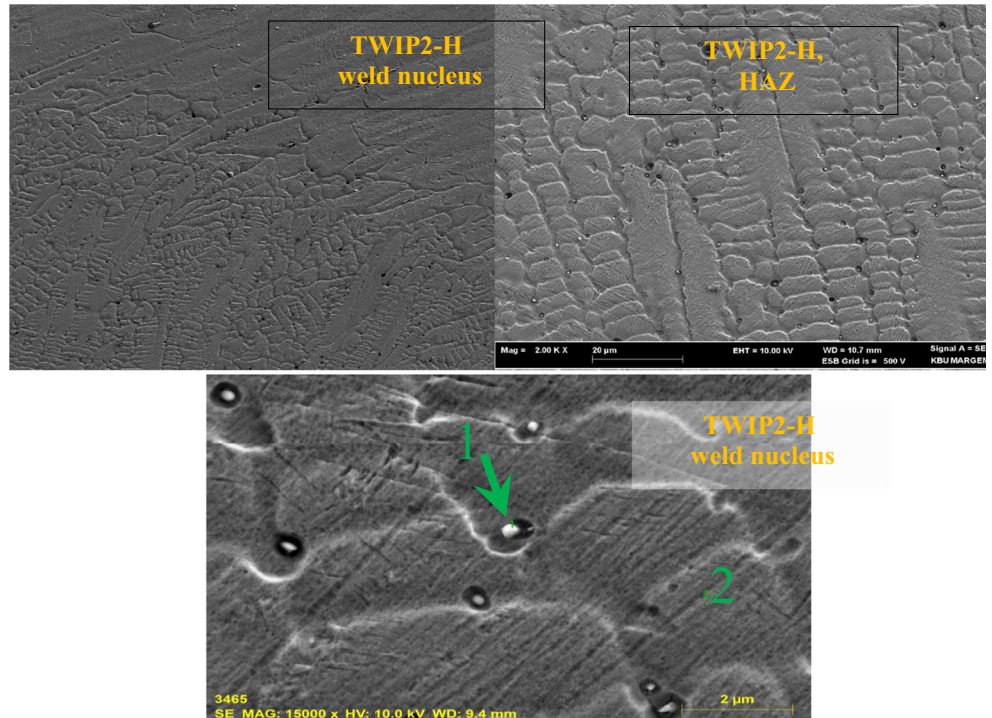
Tensile shear test results of welded samples are given in Fig. 9.

As illustrated in Fig. 9, the parameter that gives the highest tensile shear bearing capacity value in TWIP1 steel was 11 kA. It carried an average load of  $32.7 \pm 5$  kN. Although 7 kA was high in TWIP1-H sample, scattering was found. For this reason, 11 kA was chosen. Nine-kiloampere current value was the most suitable parameter in TWIP2 steel. Its load was  $35 \pm 5$  kN. J. Yu et al. [44] studied the welding time of the 1.4-mm-thick TWIP980 steel they bought commercially and the tensile shear strength and the change of heat input.

As a result of tensile shear tests, breakage patterns differed. The spot weld rupture was characterized by the destruction in the spot weld (nugget) or in the sheet. Broken images of the welded samples are given in Fig. 10.

When the welding nugget is examined, it is observed as separation with type of rupture that occurs at low welding current intensities (3 kA and 5 kA), whereas it is observed as the knob-type rupture occurs at 9–11 kA welding current intensities. Tearing-type ruptures occurred at high current intensities (13 kA). In addition, gushes have occurred due to excessive heat input and melting. The gushes are the outflow of the liquid in the core. Its content is molten metal. These rupture types and diving depths are evaluated; it is estimated that the reason for the separation-type rupture at low welding current intensities occurs because the heat is not fully formed in the welding zone, whereas the rupture from sheet material at high current intensities is caused by

**Fig. 8** SEM displays and EDX analyses of TWIP2-H welded samples



Mass percent (%)

Spectrum	C	Al	Si	P	S	Cr	Mn	Fe
1	12.33	0.14	0.76	0.89	0.22	0.27	24.48	60.90
2	3.07	0.20	0.70	0.00	0.04	0.38	14.10	81.51
Mean value:	7.70	0.17	0.73	0.45	0.13	0.33	19.29	71.21
Sigma:	6.55	0.04	0.04	0.63	0.13	0.08	7.34	14.57
Sigma mean:	4.63	0.03	0.03	0.45	0.09	0.05	5.19	10.30

excessive heat build-up. Again, it was observed that there were deep electrode traces (indentation depth) and combustion grooves at the interfaces of the assembled

parts at high current intensities and colorations on the core surface. This is thought to cause reduction and tears in tensile-shear strength.

**Table 2** Specimen sheets nugget photographs of resistance spot welded specimens

Code	Weld current				
	5kA	7kA	9kA	11kA	13kA
TWIP1					
TWIP2					



**Table 3** The nugget diameter, nucleus, and indentation depth of welded samples

Parameters	TWIP1					TWIP1-H				
	Nugget diameter	Nucleus 1	Nucleus 2	Indentation Depth 1	Indentation Depth 2	Nugget diameter	Nucleus 1	Nucleus 2	Indentation Depth 1	Indentation Depth 2
5 kA	12.5	8.55	8.35	0.35	0.3	12.5	8	8.5	0.3	0.2
7 kA	12.6	8.5	8.55	0.55	0.3	12.8	8.3	8.5	0.55	0.25
9 kA	12.6	8.4	8.6	0.6	0.35	12.5	8.25	8.25	0.35	0.2
<b>11 kA</b>	11.8	8.5	8.4	0.55	0.25	12.8	8.2	8.3	0.45	0.2
13 kA	12.5	8.3	8.4	0.55	0.3	12.2	8.3	8.5	0.4	0.3
Parameters	TWIP2					TWIP2-H				
	Nugget diameter	Nucleus 1	Nucleus 2	Indentation Depth 1	Indentation Depth 2	Nugget diameter	Nucleus 1	Nucleus 2	Indentation Depth 1	Indentation Depth 2
5 kA	12.6	8.2	8.3	0.5	0.25	12.45	8.2	8.2	0.45	0.25
7 kA	12.35	7.8	8.2	0.55	0.25	12.65	8	8	0.5	0.2
9 kA	12.2	8	8.1	0.6	0.27	12.3	7.7	8.2	0.5	0.2
<b>11 kA</b>	12.35	8.3	8.6	0.5	0.3	12.4	8.1	8	0.5	0.25
13 kA	12.4	8.4	8.25	0.45	0.25	12.2	8.7	9	0.45	0.25

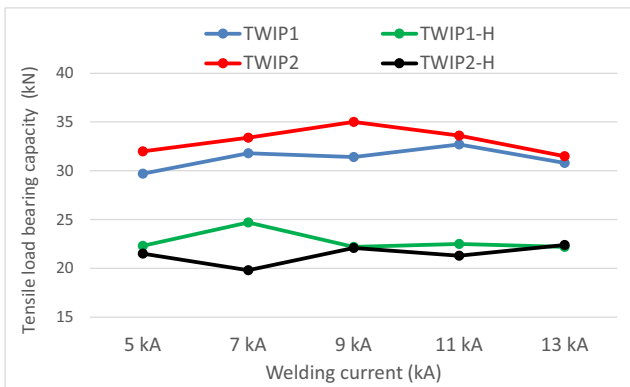


**Fig. 9** Tensile-shear testing results

### 3.6 Fracture surface SEM/EDS analysis results

SEM examinations of TWIP1 broken parts were made (Figs. 11 and 14).

In the figure, dendrite structures are clearly seen in the fracture zone. These fragmented structures reduce their strength properties. SEM examinations and EDX analyses of TWIP1 heat-treated broken pieces were performed (Fig. 12).

Dendrite structures and plastering areas were seen as seen in the photographs. In EDS analysis, it was seen that the C% values were much higher than the base metal. The C ratio was measured as 3.18% in the plastering area and 2.22% in the

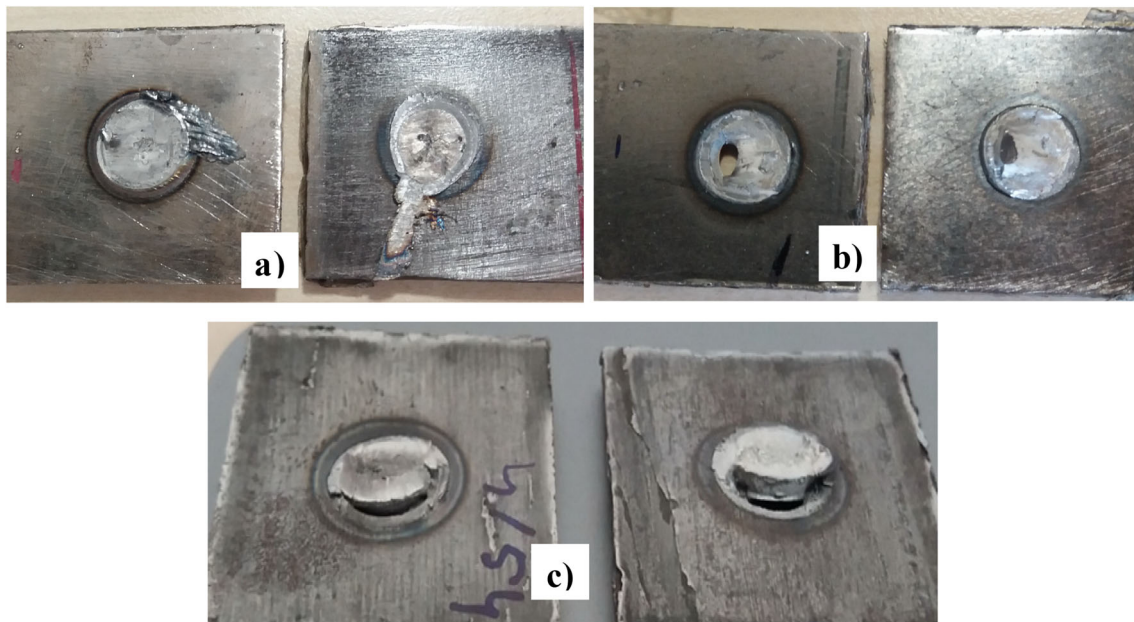


**Fig. 10** The shearing forms of welded samples: **a** Outburst displays, **b** partly partially ruptured, and **c** shearing in nugget form

**Fig. 11** SEM displays of ruptured surface

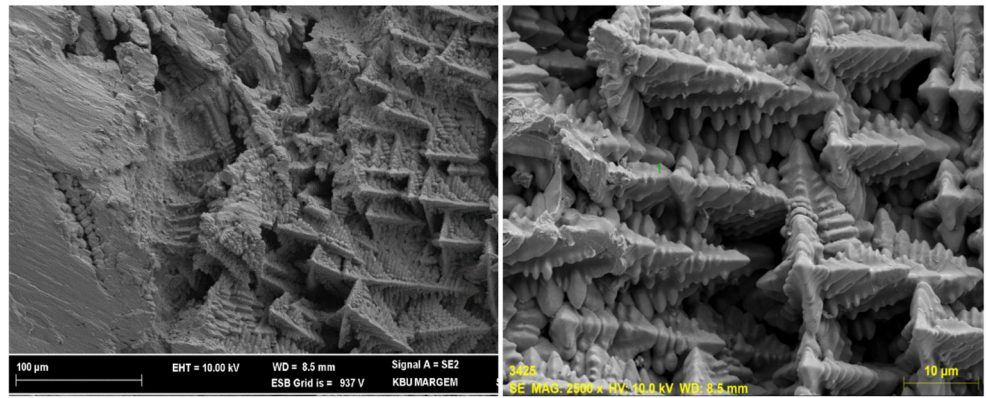
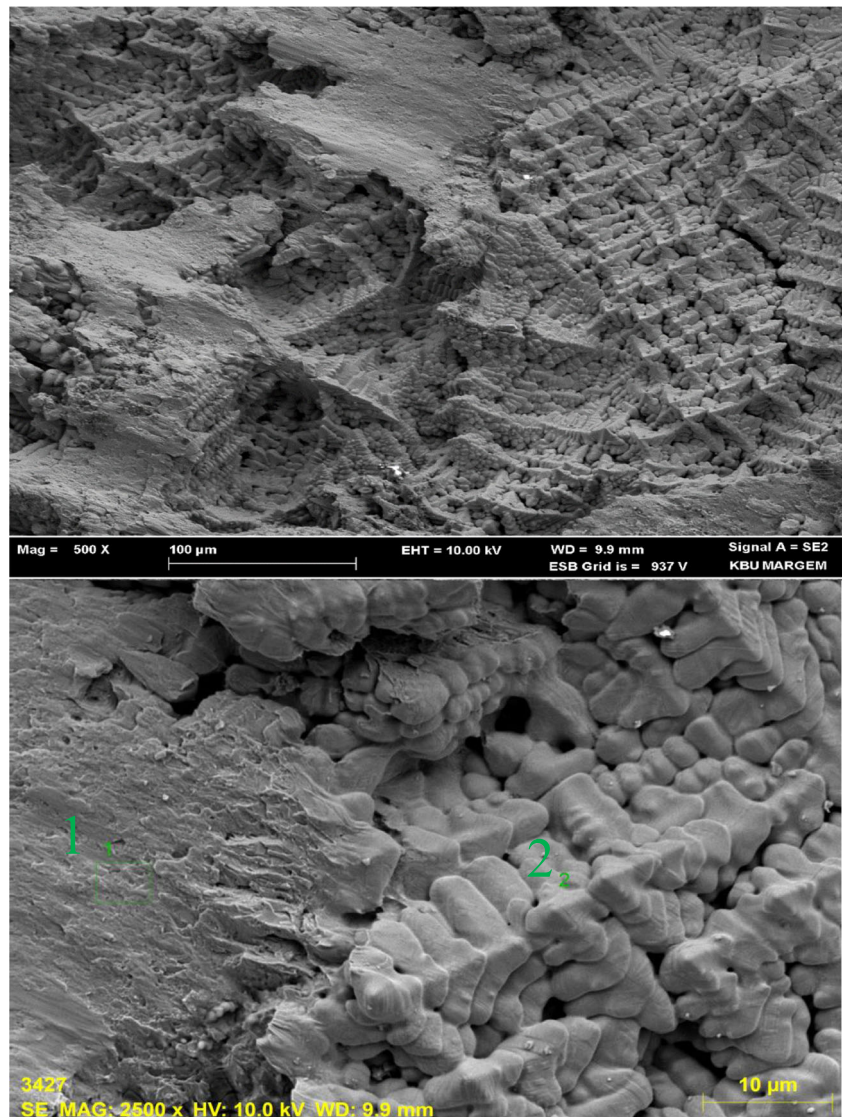


**Fig. 12** SEM displays and EDS analyses of TWIP1 welded samples

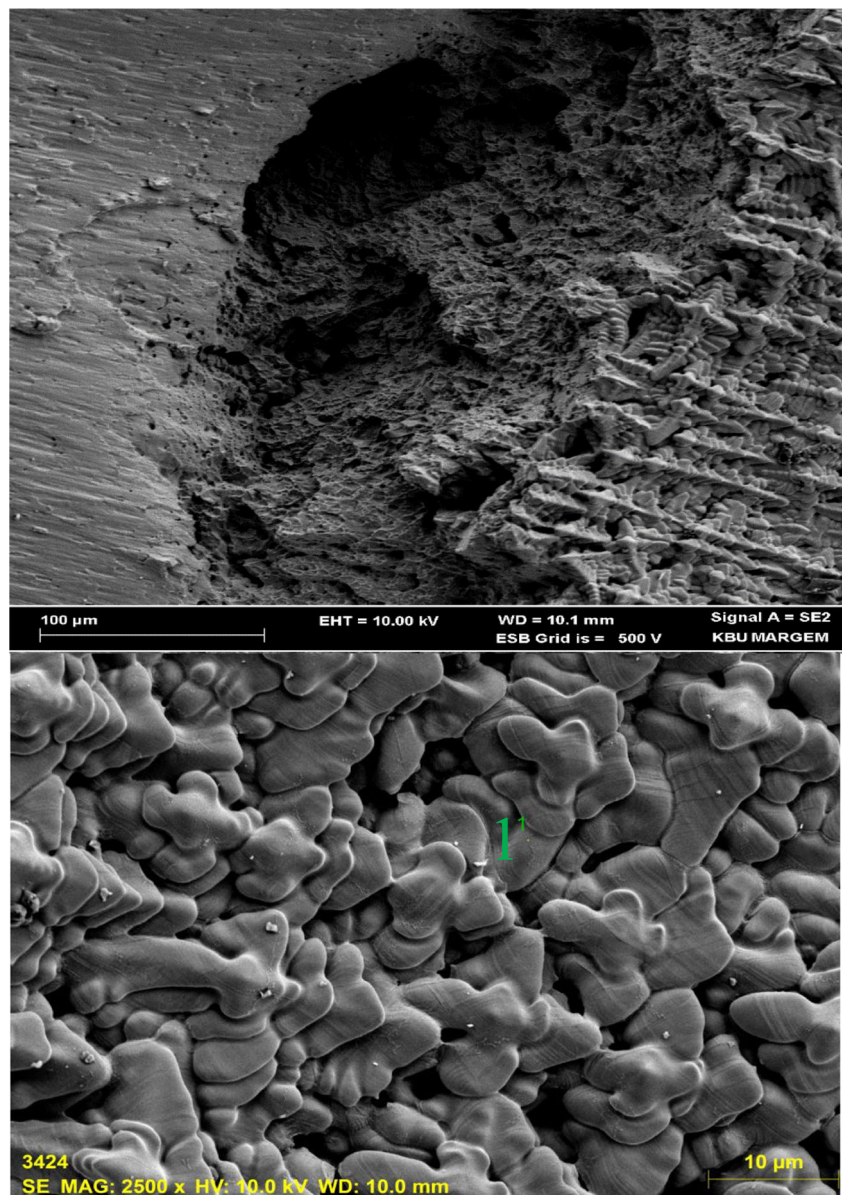


Mass percent (%)

Spectrum	C	Al	Si	P	S	Cr	Mn	Fe
1	3.18	0.60	2.08	0.00	0.16	0.18	14.71	79.09
2	2.22	0.40	1.25	0.00	0.08	0.27	15.28	80.49



**Fig. 13** SEM displays and EDS analyses of TWIP2 welded samples



El	AN	Series	unn. C [wt.%]	norm. C [wt.%]	Atom. C [at.%]	Error (1 Sigma) [wt.%]
C	6	K-series	3.44	3.35	13.72	0.74
O	8	K-series	0.00	0.00	0.00	0.00
Al	13	K-series	0.32	0.32	0.57	0.05
Si	14	K-series	0.68	0.66	1.16	0.07
P	15	K-series	0.03	0.03	0.04	0.03
S	16	K-series	0.09	0.09	0.13	0.03
Cr	24	K-series	0.00	0.00	0.00	0.00
Mn	25	K-series	16.51	16.09	14.40	0.81
Fe	26	K-series	81.55	79.47	69.97	3.80
Total:			102.62	100.00	100.00	

dendrite area. SEM investigations and EDS/EDX analysis of TWIP2 broken pieces were performed (Fig. 13).

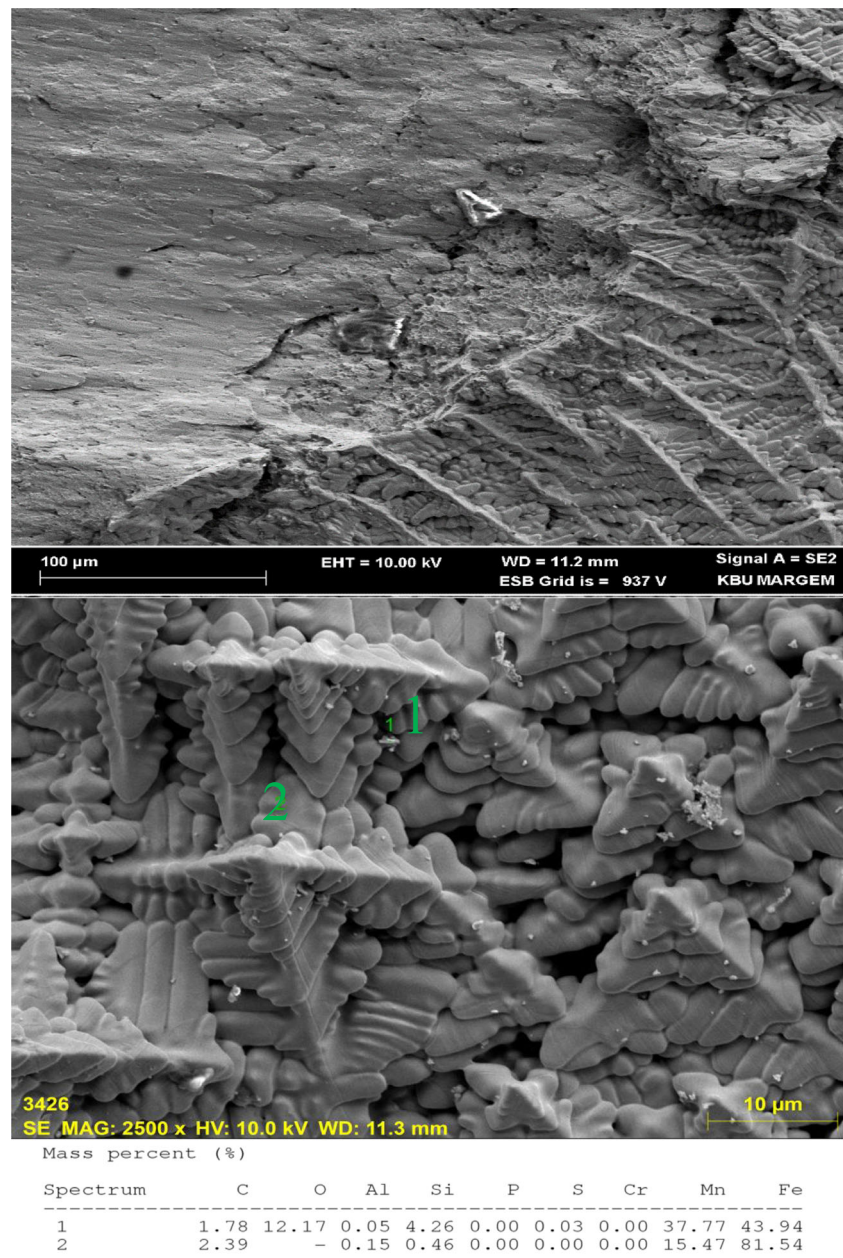
Dendrite structures separated from each other and plastering areas are seen in Fig. 13. These photos are taken from the fracture zone in Fig. 10. Intense dendrite structures were found. C ratio was found to be high in EDX analysis. SEM investigations and EDS/EDX

analyses of TWIP2 heat-treated broken pieces were performed (Fig. 14).

In Fig. 14, the % C ratio in EDX results was measured as 1.78% and 2.39. It was noteworthy that the Mn ratio increased to 37.77% at the point 1. Si ratio increased to 4.26%.

Dulal Chandra Saha et al. [35] examined the roles of the crack formations and the elements in the weld metal and HAZ

**Fig. 14** SEM displays and EDS analyses of TWIP2-H welded samples



in the resistance spot welding process of 1.4-mm-thick TWIP steel and he reported that Al and Ti have an active role in addition to the main elements (Fe, Mn, C). He also stated that Fe and Mn increase  $M_3C$  formation. This has been shown to promote crack formation. Akinay and Hayat [45] reported in their study that carbide deposits with high manganese and medium carbon ratios increased due to the increase of annealing temperature.

### 3.7 Hardness test results

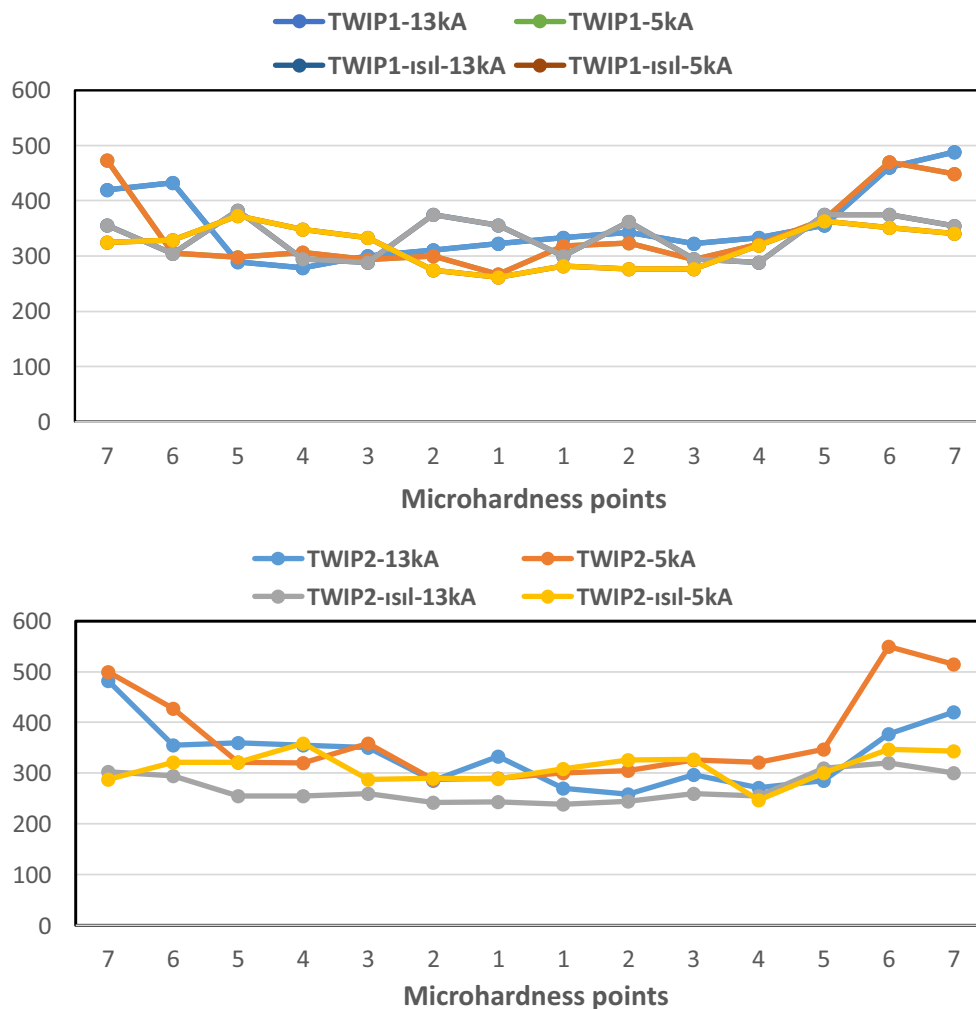
Microhardness charts, where the highest and lowest welding parameters of TWIP1 and TWIP2 steels are used, are given in

Fig. 15. Here, it is aimed to investigate the effects of parameter difference on hardness values.

The main metal hardness varied. Especially, cold-rolled TWIP1 and TWIP2 steels are at the highest value. Hardness values decreased in heat-treated samples. The graphs show that the hardness values decrease as the transition from the main metal to the HAZ and the weld core. This is due to the increase in the grain size due to the temperature effect.

M. H. Razmpoosh et al. [36] examined the mechanical, hardness, and microstructural properties of the resistance spot welding of Fe – 31Mn – 3Al – 3Si TWIP steel. It was observed that the hardness values were around 300 HV in the





**Fig. 15** Microhardness graphics for highest and lowest welding current parameters of the four sample groups

weld core center and decreased below 250 HV in HAZ. It was reported to increase to 260 or 270 HV as it gets closer to the main metal. O. Holovenko et al. [37] stated that the hardness values in the resistance spot welded joints of 18% Manganese steel varied between approximately 220 and 260 HV. It was observed that the main metal hardness value was 230–240 HV. The welding area is the region where the hardness change is greatest. It has been reported that the values of the same materials are more stable in the laser welding and the hardness in the welding center is at the lowest level as approximately 220 HV. It has been reported that the hardness has reached the highest level and increased to 250 HV in HAZ. Tao Wang et al. [31] used laser welding in 18.8% Mn steel in their study. He reported that the lowest hardness was below 240 HV in the weld metal and the main metal hardness was above 280 HV. They emphasized that it varied between 245 and 255 HV in HAZ. P Podany et al. [30] examined the hardness values of cold-rolled and heat-treated TWIP steels in laser welding of

steels with 15% Mn and two different Al contents. They reported that the hardness of the base metal was about 500 HV at the welding of the cold-rolled samples, while the hardness of the base metal with heat treatment was less than 300 HV. They stated that the lowest hardness value in the welded connection of the cold-rolled sample is in the weld metal, while in HAZ, an increase in hardness is observed from the area close to the weld center to the main metal. They stated that the welding hardness of the heat-treated sample is different. It is reported that the hardest area reaching 350 HV is in the weld metal. It has been observed that there is a balanced hardness change in basic metal and HAZ. Li-li MA et al. [40] compared TIG and Laser welding of 24% Mn TWIP steel. In the welded joint made with the TIG method, they reported that the hardness of the weld metal was measured variably below and above 340 HV and the average was 300 HV. He reported that it exceeded 420 HV in the laser welding and the average value was 400 HV.

## 4 Conclusion

In this study, the point resistance welding properties of TWIP steels in two different chemical compositions were investigated. As a result of the work done:

- (1) The highest tensile strength in the produced steels was achieved in TWIP1 steel without heat treatment. The highest elongation value as percentage was seen in the heat-treated sample of TWIP2-H steel.
- (2) In welding processes, shrinkage gaps have occurred with increasing welding current. These macro-level gaps increase due to increased heat input. In particular, a significant increase and growth in 13-kA weld current value was observed in gap formation. Sufficient connections have not been established in 3 kA.
- (3) With the increased welding current, there was an increase in gushes in the melting zone. This increase causes mass loss in the welding core.
- (4) It was determined that dendritic structures were formed in the nucleus region where melting occurred. It was observed that the grain size increased in HAZ. In addition, in some samples, gaps and pores were detected between the dendrites. The reason for this is the high solidification shrinkage occurring in the regions between the dendrites.
- (5) It has been determined that there is a decrease in micro hardness values in HAZ. The reason for this is the grain growth from thermal cycle.
- (6) In the fracture surface images, it was determined that the welding nucleus center consists of dense dendrite structures. In the EDS analysis, it was found that especially the carbon element increased exponentially and played a role in breakage.

**Acknowledgements** We would like to thank TÜBİTAK (Project Scientific and Technological Research Council of Turkey) for their support for the project number 115M112 within the scope of the initial R&D project.

## References

1. Keil D, Zinke M, Pries H (2011) Weldability of novel Fe-Mn high-strength steels for automotive applications. *Weld World* 55:1–10
2. Ivanjkol M, Meschut G (2019) Innovative joining technology for multi-material applications with high manganese steels in light-weight car body structures. *Weld World* 63:97–106
3. Sezgin CT (2017) Importance of using new generation steel in automotive industry. *Acad J Eng Appl Sci* 1(3):205–210
4. Sezgin CT, Hayat F (2020) Microstructure and mechanical behavior of TRIP 800 and DP 1000 steels welded by electron beam welding method. *Soldagem Inspeção* 25(1):1–12
5. Hu B, Luo H, Yang F, Dong H (2017) Recent progress in medium-Mn steels made with new designing strategies: a review. *J Mater Sci Technol* 33(12):1457–1464
6. Ofei KA, Zhao L, Sietsma J (February 2013) Microstructural development and deformation mechanisms during cold rolling of a medium stacking fault energy TWIP steel. *J Mater Sci Technol* 29(2):161–167
7. Kim HJ, McMillan C, Keoleian GA, Skerlos SJ (2010) Greenhouse gas emissions payback for lightweighted vehicles using aluminum and high-strength steel. *J Ind Ecol* 14:929–946
8. Onar V, Özen F, Kekik M (May 2019) Yusuf Sadi Aslanlar, Yüksel Özderin, Hacı Aslan & Salim Aslanlar, Effect of current and welding time on tensile-peel strength of resistance spot welded TWIP 1000 and martensitic steels. *Indian J Chem Technol* 26: 248–251
9. Wittig B, Zinke M, Jüttner S, Keil D (2019) A new constitution diagram for dissimilar metal welds of high-manganese steels. *Weld World* 63:491–499
10. Saha DC, Cho Y, Park Y-D (2013) Metallographic and fracture characteristics of resistance spot welded TWIP steels. *Sci Technol Weld Join* 18(8):711–720
11. Allain S, Chateau J-P, Bouaziz O, Migot S, Guelton N (2004) Correlations between the calculated stacking fault energy and the plasticity mechanisms in Fe–Mn–C alloys. *Mater Sci Eng A* A387–A389:158–162
12. Keil D, Zinke M and Pries H, (2011) Weldability of novel Fe-Mn high-strength steels for automotive applications. *Welding World* 12 (55).
13. Liqing C, Yang Z, Xiaomei Q (2013) Some aspects of high manganese twinning-induced plasticity (TWIP) steel. *Acta Metall Sin (Engl Lett)* 26(1):1–15
14. Chung K, Maa N, Park T, Kim D, Yoo D, Kim C (2011) A modified damage model for advanced high strength steel sheets. *Int J Plast* 27:1485–1511
15. Haase C, Ingendahl T, Güvenç O, Bambach M, Bleck W, Molodov DA, Luis A, Barrales-Mora (2016) On the applicability of recovery-annealed twinning-induced plasticity steels: potential and limitations. *Mater Sci Eng A* A649:74–84
16. Sun DQ, Lang B, Sun DX, Li JB (2007) *Mater Sci Eng A* 460–461: 494–498
17. AWS. (1991) *Welding Processes, Welding Handbook Vol. 2, 8th ed.* Miami: AWS
18. (1999) *Safety and Health Fact Sheet no. 21*, American Welding Society.
19. H. Zhang and J. Senkara: ‘Resistance welding – fundamentals and applications’; 2006, London, Taylor & Francis/CRC Press.
20. Hayat F. (2011) *J Iron Steel Res Int* 18:70. [https://doi.org/10.1016/S1006-706X\(12\)60037-5](https://doi.org/10.1016/S1006-706X(12)60037-5).
21. Aslanlar S (2006) The effect of nucleus size on mechanical properties in electrical resistance spot welding of sheets used in automotive industry. *Mater Des* 27:125–131
22. Fatih H (2012) Effect of aging treatment on the microstructure and mechanical properties of the similar and dissimilar 6061-T6/7075-T651 RSW joints. *Mater Sci Eng A* 556:834–843
23. Hayat F, Sezgin CT, Şerifoğlu A Investigation of fracture surface of different metals welded by resistance spot welding. *J Mater Electronic Devices* 1(1):45–49
24. Sevim I, Hayat F, Kulekci MK Nucleus geometry and mechanical properties of resistance spot welded coated-uncoated DP automotive steels. *Bull Mater Sci* 36(6):1049–1055
25. Brauser S, Pepke LA, Weber G, Rethmeier M (2010) *Mater Sci Eng A* 527:7099–7108
26. Radakovic JD, Tumuluru MD, (2008) In: *Proceedings of the International Sheet Metal Welding Conference XIII*.
27. Mújica L, Weber S, Theisen W (2012) Welding of twinning-induced plasticity steels. *Scr Mater* 66:997–1001
28. Dahmen M, Lindner S, Monfort D, Petring D (2016) Weld metallography and mechanical properties of high manganese ultra-high strength dissimilar welds. *Phys Procedia* 83:344–351



29. Podany P, Koukolikova M, Kubina T, Prochazka R, Franc A (2017) Fe-Mn(Al, Si) TWIP steel – strengthening characteristics and weldability. *Mater Sci Eng* 179:012057. <https://doi.org/10.1088/1757-899X/179/1/012057>
30. Spena PR, Rossini M, Cortese L, Matteis P, Scavino G, Firrao D, (2015) Laser welding between TWIP steels and automotive high-strength steels, *Charact Miner Met Mater*
31. Wang T, Zhang M, Xiona W, Liu R, Shi W, Lin L (2015) Microstructure and tensile properties of the laser welded TWIP steel and the deformation behavior of the fusion zone. *Mater Des* 83:103–111
32. Behma V, Höfemann M, Hatscher A, Springer A, Kaierle S, Hein D, Otto M, Overmeyer L (2014) Investigations on laser beam welding dissimilar material combinations of austenitic high manganese (FeMn) and ferrite steels. *Phys Procedia* 56:610–619
33. Rossini M, RussoSpena P, Cortese L, Matteis P, Firrao D (2015) Investigation on dissimilar laser welding of advanced high strength steel sheets for the automotive industry. *Mater Sci Eng A* 628:288–296
34. Yu J, Shim J, Rhee S (2012) Characteristics of resistance spot welding for 1 GPa grade twin induced plasticity steel. *Mater Trans* 53(11):2011–2018
35. Saha DC, Chang IS, Park Y-D (2014) Heat-affected zone liquation crack on resistance spot welded TWIP steels. *Mater Charact* 93:40–51
36. Razmpoosh MH, Shamanian M, Esmailzadeh M (2015) The microstructural evolution and mechanical properties of resistance spot welded Fe–31Mn–3Al–3Si TWIP steel. *Mater Des* 67:571–576
37. Holovenko O, Ienco MG, Pastore E, Pinasco MR, Matteis P, Scavino G, Firrao D (2013) Microstructural and mechanical characterization of welded joints on innovative high-strength steels. *La Metallurgia Italiana* 105(3):3–12 2-12
38. Ashiri R, Haque MA, Ji C-W, Shamanian M, Salimijazi HR, Park Y-D (2015) Supercritical area and critical nugget diameter for liquid metal embrittlement of Zn-coated twinning induced plasticity steels. *Scr Mater* 109:6–10
39. Onar V, Özen F, Kekik M, Aslanlar YS, Özderin Y, Aslan H, Aslanlar S (2019) Effect of current and welding time on tensile-peel strength of resistance spot welded TWIP 1000 and martensitic steels. *Indian J Chem Technol* 26:248–251
40. Li-li MA, Wei Y-G, Hou L-f, Yan B (2014) Microstructure and mechanical properties of TWIP steel joint. *J Iron Steel Res Int* 21(8):749–756
41. Russo Spena P, Matteis P, Sanchez A, Scavino G, (2013) Strength and fracture of TWIP steel dissimilar weld joints, P. Russo Spena et al. Roma, Italia, 1-3 Luglio, ISBN 978-88-95940-47-2.
42. Kang S, Junga YS, Junb JH, Lee YK (2010) Effects of recrystallization annealing temperature on carbide precipitation microstructure, and mechanical properties in Fe–18Mn–0.6C–1.5Al TWIP steel. *Materials Science & Engineering A*. A 527:745–751
43. Yoo J, Kim S, Park Y, Choi J, Lee C, (2011) Characteristics of the hot cracking and segregation behavior in the high manganese steel, In: *Proceedings of the 1st International Conference on High Manganese Steels*, Seoul. p. F-7.
44. Yu J, Choi D, Rhee S (2014) Improvement of weldability of 1 GPa Grade twin-induced plasticity steel. *Weld Res* 93:78s–84s
45. Akinay Y, Hayat F (2016) The influence of the heat treatment on mechanical and microstructure properties of Fe-Mn-C high-manganese steel. *Kov Mater* 54:1–6

**Publisher's note** Springer Nature remains neutral with regard to jurisdictional claims in published maps and institutional affiliations.